

Large flow shears around auroral beads at substorm onset

K. Hosokawa,^{1,2} S. E. Milan,³ M. Lester,³ A. Kadokura,⁴ N. Sato,⁴ and G. Bjornsson⁵

Received 18 August 2013; revised 12 September 2013; accepted 12 September 2013; published 1 October 2013.

[1] We present a fine-scale electrodynamic structure behind the auroral beads observed immediately before substorm onset, as inferred from high spatial and temporal resolution measurements of substorm with an all-sky TV camera (ATV) and a coherent high frequency radar of Super Dual Auroral Radar Network in Iceland. On the night of 24 September 2006, the ATV observed eastward propagating auroral beads in the initial brightening arc of a substorm just prior to the poleward expansion. During the sequential passage of the beads across the radar beams, the radar detected large velocity flow shears whose magnitude was in excess of 0.27 s^{-1} . The observations suggest that flow shears were located very close to the center of the beads; thus, they corresponded to electric fields converging toward the beads, which is consistent with the existence of upward field-aligned currents (FACs) flowing out of the beads. The temporal and spatial resolutions of the current radar measurement were still insufficient for fully resolving the detailed electrodynamic structure behind the fast moving auroral beads. At least, however, we can suggest the existence of highly localized filamentary FAC structures behind the beads, which would be an important consequence of possible plasma instabilities operating in the M-I coupling region or near the equatorial plane of the magnetosphere. **Citation:** Hosokawa, K., S. E. Milan, M. Lester, A. Kadokura, N. Sato, and G. Bjornsson (2013), Large flow shears around auroral beads at substorm onset, *Geophys. Res. Lett.*, *40*, 4987–4991, doi:10.1002/grl.50958.

1. Introduction

[2] The onset of auroral breakup is characterized by a sudden increase in the brightness of a preexisting or newly formed initial brightening arc (IBA) and by subsequent poleward progression of the arc. Recently, the temporal evolution of the IBA, in the few minutes before the expansion, has drawn attention because it could illustrate the processes causing the onset of substorms. *Donovan et al.* [2006] first reported an IBA that consisted of propagating bright spots like beads with a wavelength of $\sim 100 \text{ km}$ and an azimuthal propagation speed of $\sim 5 \text{ km s}^{-1}$. Since then, such bead-

ing structures have been called “auroral beads” and studied by many authors [e.g., *Liang et al.*, 2008; *Sakaguchi et al.*, 2009]. Recently, *Motoba et al.* [2012] showed that magnetic conjugacy of auroral beads is generally good and claimed that they are a manifestation of plasma instabilities in the magnetosphere. However, they also pointed out that there existed a certain level of interhemispheric dissimilarities in the evolution of the beads, implying a contribution of the processes in the M-I coupling region.

[3] To discuss the processes creating auroral beads in detail, it is necessary to observe the plasma flow and corresponding field-aligned current (FAC) structure behind them, for example, as visualized by *Wescott et al.* [1975] through observations of Barium releases from a rocket. However, the spatial scale of the beads is an order of a few tens of kilometers and, in addition, they move very fast [e.g., *Sakaguchi et al.*, 2009], which has not allowed ground-based radars to resolve such structures. For instance, *Voronkov et al.* [1999] investigated combined Super Dual Auroral Radar Network (SuperDARN) and optical observations of preonset auroral structures. At that time, however, it was difficult to identify small-scale structures in the plasma flow due to the limited temporal resolution of the radar. We have addressed this issue by conducting simultaneous high-spatiotemporal resolution measurements of IBA by an all-sky TV camera and a coherent high frequency radar of SuperDARN in Iceland. Although the spatial and temporal resolutions are still not enough to fully resolve the dynamic behavior of the IBA, some interesting electric field structures have been identified within the longitudinally propagating beads, which are discussed here in terms of the structuring process of the IBA immediately before the expansion phase onset.

2. Experimental Arrangement

[4] We employed a white-light all-sky TV (ATV) camera at Tjörnes (66.20°N , 17.12°W) and a SuperDARN radar at Pykkvibær (63.77°N , 20.54°W) in Iceland. The ATV recorded auroral images at a rate of 29.97 frames per second. The field of view (FOV) of the ATV shown in Figure 1 is mapped, assuming that the altitude of optical emission is 110 km. The radar sounds along 16 different beam directions (beams 0 to 15) separated by 3.24° in azimuth, with the radar boresite pointing at an azimuth of 30° clockwise from north. Radar echoes are gated into 75 range bins, usually of 45 km in length, with a range of 180 km to the first gate. During the present observation, however, the observing mode was optimized for resolving auroral beads by reducing the gate length to 15 km and concentrating soundings to closer ranges, which is known as the “myopic” mode. This reduced FOV is displayed in Figure 1. In addition to the improvement of the spatial resolution by the myopic mode, the “stereo” capability allowed the radar to sound in two different look directions in the two stereo channels (Channels A and B)

¹Department of Communication Engineering and Informatics, University of Electro-Communications, Tokyo, Japan.

²Center for Space Science and Radio Engineering, University of Electro-Communications, Tokyo, Japan.

³Department of Physics and Astronomy, University of Leicester, Leicester, UK.

⁴National Institute of Polar Research, Tokyo, Japan.

⁵Science Institute, University of Iceland, Reykjavik, Iceland.

Corresponding author: K. Hosokawa, Department of Communication Engineering and Informatics, University of Electro-Communications, Tokyo, Japan. (keisuke.hosokawa@uec.ac.jp)

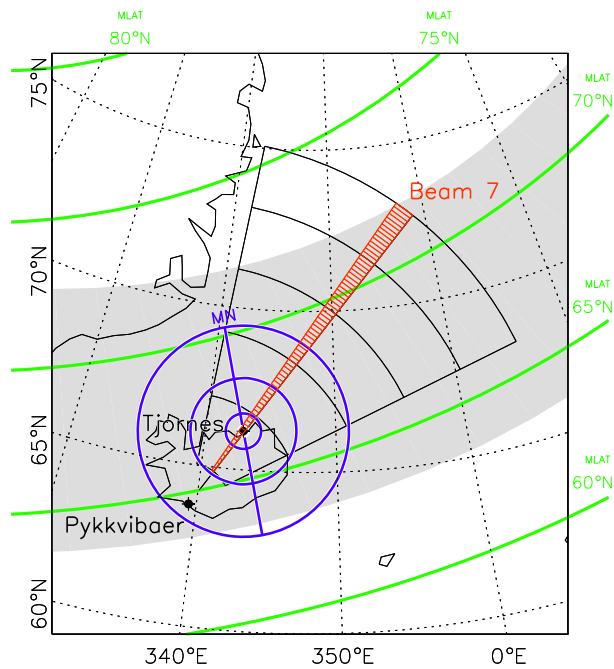


Figure 1. A map showing the FOV of the SuperDARN radar at Pykkvibaer and the all-sky TV camera at Tjornes. The radar FOV is mapped, assuming a backscatter altitude of 160 km. The projection of the FOV of the ATV is shown, the four concentric circles marking the loci of zenith angles of 30°, 60°, and 75° mapped to an altitude of 110 km.

almost simultaneously. In the “stereo myopic” mode, the 16 beams were scanned clockwise from beam 0 to beam 15 in Channel A with a dwell time of 2 s each. Thus, a full scan of the FOV was completed every 34 s. In Channel B, the radar always scanned along beam 7 (shown in red in Figure 1) looking over the zenith of Tjornes, with a dwell time of 2 s. This enabled us to detect rapid variations of the ionospheric plasma drift without losing the two-dimensional distribution of radar backscatter.

3. Observations

[5] On the night of 24 September 2006, a small substorm was captured by the ATV at Tjornes in the premidnight sector. Figure 2 shows a sequence of cropped all-sky images selected at 15 s intervals from the appearance of the IBA to the start of the poleward expansion. At 22:37:45 UT, the arc appeared from the west and subsequently progressed eastward very rapidly. During this longitudinal progression, the arc showed several small-scale swirling spots, which look similar to the auroral beads reported previously [e.g., *Donovan et al.*, 2006]. The beads propagated eastward and finally led to the poleward expansion at 22:39:00 UT. In the lower five panels, some of the beads are marked by arrows for better showing their eastward propagation. We estimated the speed of the beads in the longitudinal direction to be ~ 3 km through close investigation of successive images. The spatial scale of the beads was not constant, but the separation between the neighboring spots was 50–70 km. These values are consistent with the earlier observations by *Sakaguchi et al.* [2009].

[6] Figure 3a shows the optical data at 22:38:29 UT, as mapped onto the polar geomagnetic coordinate system,

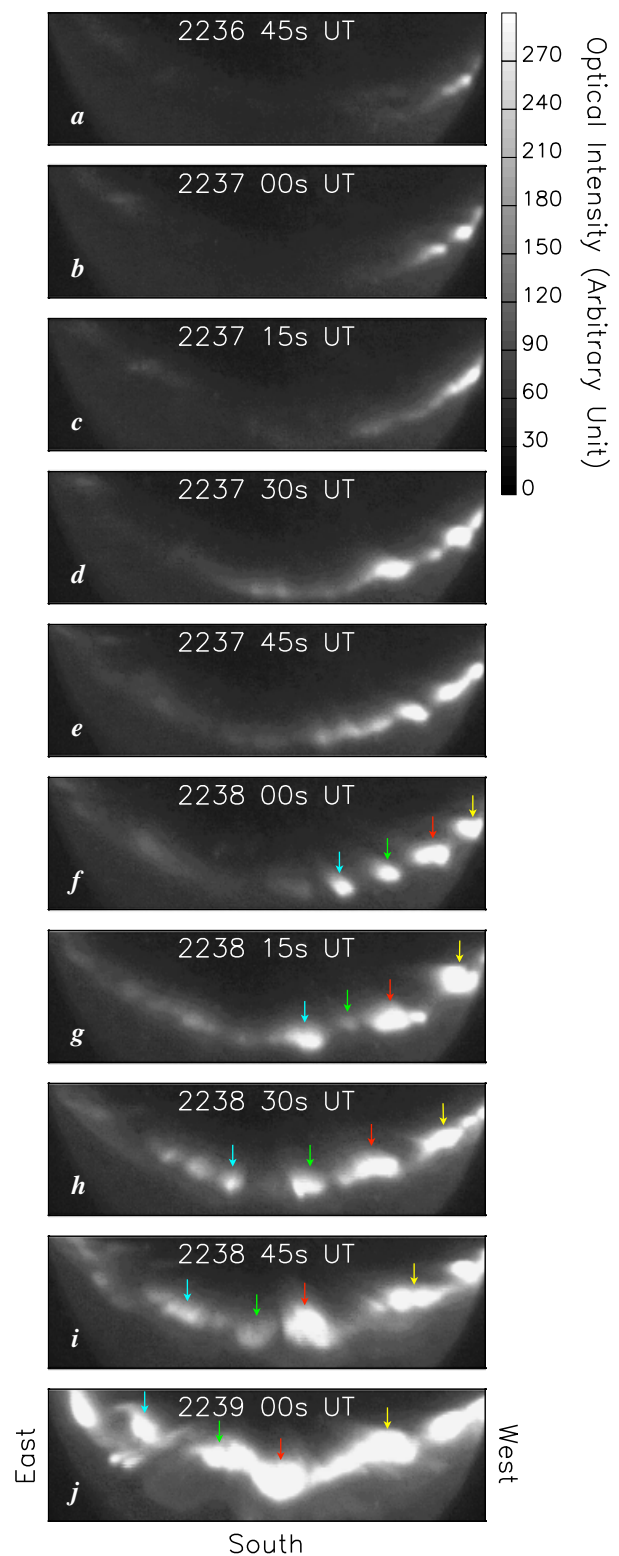


Figure 2. (a–j) Sequence of cropped all-sky images selected at 15 s intervals from the appearance of the initial brightening arc to the start of the poleward expansion (from 22:36:45 UT to 22:39:00 UT).

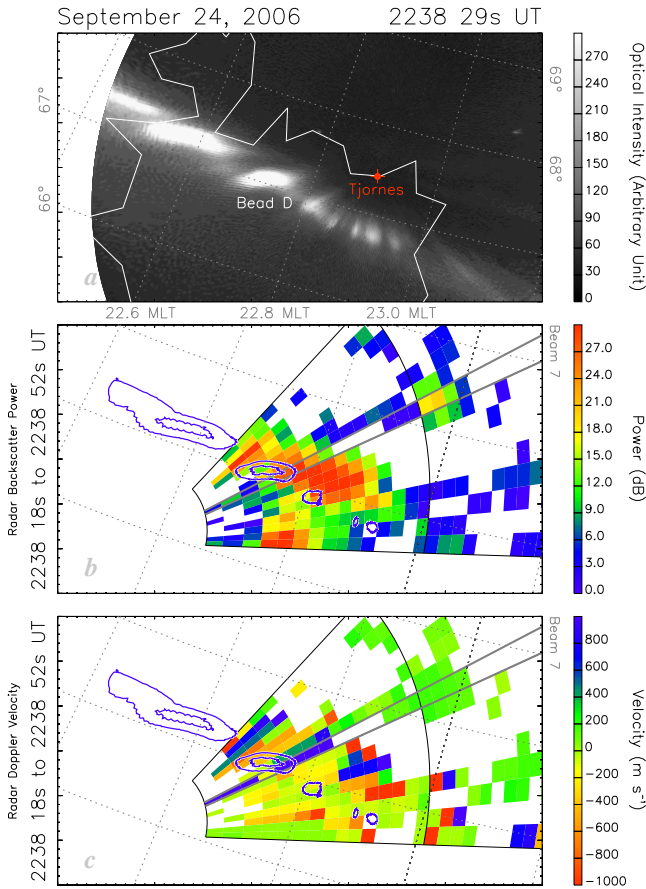


Figure 3. (a) Optical data at 22:38:29 UT, (b) backscatter power and (c) Doppler velocity obtained simultaneously from the full scan in Channel A, respectively. For comparison purpose, the spatial distribution of the auroral beads is shown as the blue contours.

in which the auroral beads were clearly observed within the IBA. The overlaid grids indicate magnetic latitude and magnetic local time. The backscatter power obtained simultaneously from the full scan in Channel A is shown in Figure 3b. For comparison purposes, the spatial distribution of the auroral beads is superimposed as the blue contours. Stronger echoes were seen slightly poleward of the arc as an L-shell aligned region of enhanced backscatter power. Even within the arc, the radar obtained echoes whose signal-to-noise ratio was sufficiently high for estimating the Doppler shift of the radar spectra. In Figure 3c, the Doppler velocity from Channel A is shown in the same format as Figure 3b. The Doppler velocities within the arc are found to be somewhat suppressed, which is more clearly seen in the eastern beams as light greenish colors indicating velocity magnitude less than 100 m s⁻¹. Such a velocity reduction within a discrete arc is usually attributed to enhanced conductivities associated with auroral electron precipitation [e.g., *Grocott et al., 2009*]. More importantly, the velocity data exhibited strong velocity shears possibly in association with the bead structures. Such shear structures are more clearly seen slightly poleward of the arc in the western part of the FOV, where a systematic change of the sign of the velocity in the azimuthal direction is identified. One thing we have to remind is that spatial collocation between the shears and the beads was not always perfect. Since the speed of the eastward motion

of the beads was $\sim 3 \text{ km s}^{-1}$, they can travel for $\sim 100 \text{ km}$ within a scan of the radar of 34 s. The separation between the beads is an order of tens of kilometers; thus, one-to-one close correspondence between the beads and the velocity shear structures should be missing in the full scan radar data. At least, however, the current observations show an indication that the ionospheric electric field had some small-scale structures in the vicinity of the beads.

[7] We now turn to look at the Doppler velocity data from Channel B, in which we only made a measurement along beam 7 looking over the zenith of Tjörnes with a temporal resolution of 2 s, which could allow us to better resolve the small-scale velocity feature associated with the beads. Figure 4a shows a beam 7 aligned keogram reproduced from the ATV images during a 2 min interval from 22:37 to 22:39 UT. As shown in Figure 2, the IBA progressed eastward, and therefore, we observed the auroral beads passing through beam 7 sequentially. Such a sequential passage of

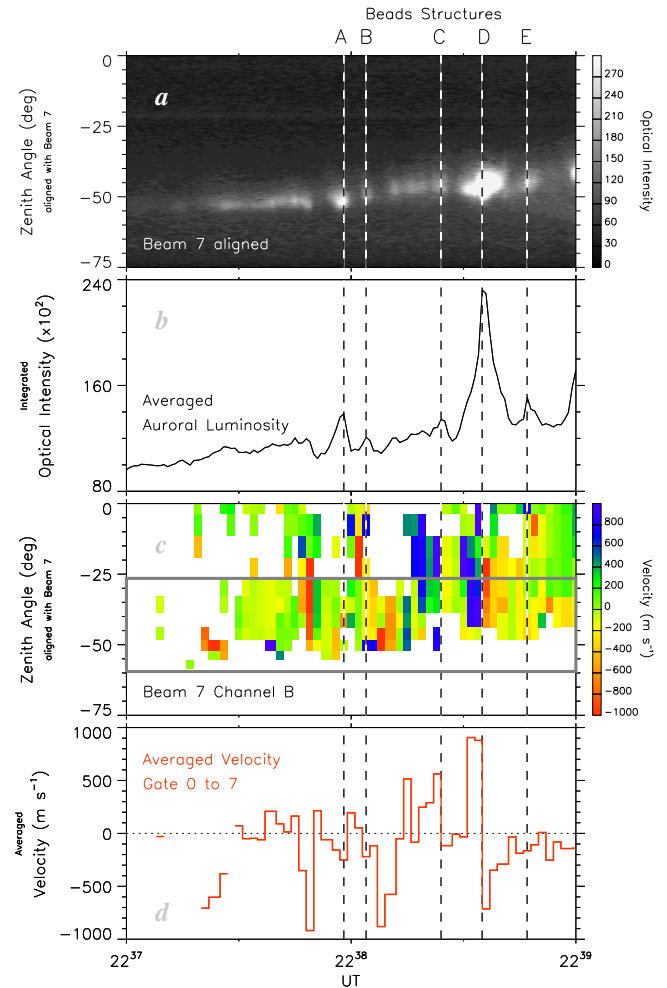


Figure 4. (a) Beam 7 aligned keogram reproduced from the ATV images during a 2 min interval from 2237 to 2239 UT. Passages of the beads are marked by the dashed vertical lines. (b) Auroral luminosities integrated over the zenith angle range shown in Figure 4a. (c) Doppler velocity from Channel B. The data are mapped onto the FOV of the ATV and plotted as a format of keogram along beam 7. (d) Temporal variation of the Doppler velocity averaged over the grey rectangle in Figure 4c.

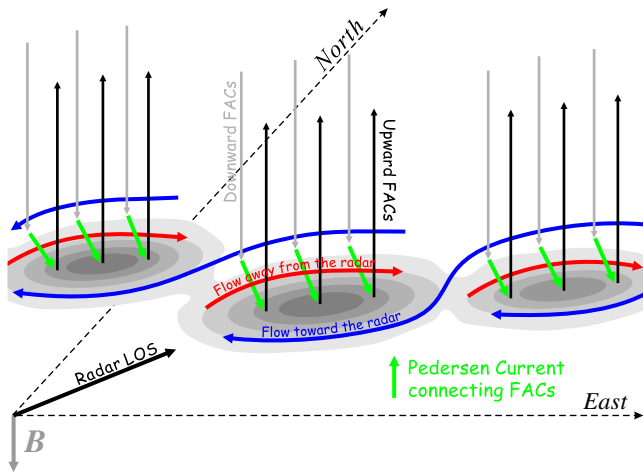


Figure 5. Schematic drawing of the electrodynamic structure behind the auroral beads.

the beads can be seen in the keogram as bright spots marked by the dashed vertical lines. Figure 4b shows the auroral luminosity integrated over the zenith angle range shown in Figure 4a. During this interval, we observed five peaks (A–E) of auroral luminosity associated with the passage of the beads. The luminosity appears to be increasing just as the time series ends; thus, one may expect another peak after 22:39 UT. However, this increase in the luminosity was caused by further brightening due to the poleward expansion, and therefore, it was not related to the passage of the beads. Bead D was brightest among the five, and this is the one accompanied by the velocity shear in Figure 3c. Figure 4c shows the Doppler velocity from Channel B, in which the radar data are mapped onto the FOV of the ATV and plotted as a format of keogram along beam 7. After the appearance of the IBA at $\sim 22:37:20$ UT, radar backscatter was observed within and slightly poleward of the arc. The Doppler velocity changed its sign quasi-periodically, especially after the first bead was observed at $\sim 22:37:58$ UT. Figure 4d shows the temporal variation of the Doppler velocity averaged over the grey rectangle in Figure 4c. The averaged velocity also changed its sign very frequently. More interestingly, at the time of beads B, C, and D, the velocity changed from positive (toward the radar) to negative (away from the radar) very sharply. In particular, when the brightest bead D was observed at $\sim 22:38:35$ UT, the radar detected a very large velocity reversal whose magnitude was in excess of 1.5 km s^{-1} . Such a velocity reversal was less clear at the time of beads A and E, which may imply that the 2 s temporal resolution of Channel B was still insufficient for fully tracking the velocity structure moving with the beads.

4. Discussion and Summary

[8] As shown in Figure 4d, the line-of-sight velocity changed from 900 to -700 m s^{-1} in 2 s when bead D passed through beam 7. Hence, the velocity change in 1 s was $\sim 800 \text{ m s}^{-1}$. Since the eastward speed of the bead was $\sim 3 \text{ km s}^{-1}$, the shear should be $\sim 0.27 \text{ s}^{-1}$ ($\sim 0.8 \text{ km s}^{-1}/3 \text{ km}$). Before the passage, the radar observed velocities toward the radar and after the passage, it observed those away from the radar. Since the IBA progressed eastward, such a temporal variation of the velocity indicates that

the toward (away) velocities were distributed in the eastern (western) part of the bead. Figure 3 also shows that the velocities toward (away from) the radar were seen in the eastern (western) side of bead D. This correspondence between the peak of the bead and the velocity shear indicates that these two structures were closely associated. Since the temporal resolution of the 2-D scan of the radar was insufficient for tracking the rapidly moving beads, we cannot make concrete conclusions about the electrodynamic structure behind the beads only from the current observations. However, we speculate the flow pattern and a FAC structure near the beads and draw schematic illustration in Figure 5. Note that this illustration is rather speculative and not fully supported by the data. The flow shear was located very close to the center of the bead. Such a velocity shear corresponds to the horizontal electric field converging toward the bead, which is consistent with upward FACs flowing out of the bead. In addition, if we take a closer look at Figure 3, another velocity shear having opposite direction can be identified in the dark area northwest of bead D (between beams 2 and 3). In Figure 5, we also depict such a flow shear in the west of the bead. This velocity structure corresponds to the diverging electric field, which is consistent with downward FACs probably carried by upwelling thermal electrons. FACs flowing out of the center of the bead and those flowing into the dark area adjacent to it were possibly connected by horizontally flowing Pedersen current indicated by the green arrows.

[9] We have shown an indication of strong velocity shear adjacent to the auroral beads, suggesting the existence of a well-structured FAC system drifting in tandem with the beads. To the best of our knowledge, such a current system associated with auroral beads has never been observed by ground-based radars. Roux *et al.* [2006] showed, by using the Cluster data, an existence of eastward propagating waves, possibly associated with the ballooning instability, in the first several minutes of the onset. They suggested that such an eastward propagating perturbation would lead to an azimuthal modulation of the cross-tail current and eventually produce localized filamentary FAC structures via $\nabla \cdot \mathbf{J} = 0$. Henderson [2009] also claimed that such filamentary FAC features can be launched from the region of ballooning instability on the equatorial plane of the magnetosphere during the formation of auroral beads. Therefore, the structures of FAC and associated plasma drift illustrated in Figure 5 are generally consistent with the mechanism based on the instabilities in the magnetosphere. However, it does not mean that the present observations rule out alternative generation process of beads. For example, recent M-I coupling simulations by Hiraki [2013] have suggested that when the background electric field is large enough, structuring of an auroral arc in the longitudinal direction can occur through the ionospheric feedback instability (IFBI) operative in the M-I coupling region. Similar filamentary FAC structures should be formed during the structuring through the IFBI process. Thus, with only the present measurements, it is still impossible to determine for certain the generation mechanism of auroral beads. In order to investigate the possible relationship between the periodic auroral structures appearing immediately before the substorm onset and corresponding plasma processes in the magnetotail or M-I coupling region, it is essential to combine further improved spatiotemporal resolution ground-based measurements like EISCAT_3D

(<https://www.eiscat3d.se>) together with well-designed computer simulations [e.g., Hiraki, 2013; Raeder et al., 2013]. The current measurements visualized a fundamental electrodynamic structure existing behind auroral beads that should be observed by the next-generation measurements and reproduced by the future computer simulations.

[10] **Acknowledgments.** This work was supported by grant-in-aid for Scientific Research (B) 21403007 under Japan Society for the Promotion of Science. The operation of the CUTLASS SuperDARN radars is funded by the RSPP group at the University of Leicester. M.L. and S.E.M. acknowledge financial support from STFC under grant ST/H002480/1 and ST/K001000/1.

[11] The Editor thanks William Bristow and Eric Donovan for their assistance in evaluating this paper.

References

- Donovan, E., et al. (2006), The azimuthal evolution of the substorm expansive phase onset aurora, in *Proceedings of ICS-8*, edited by M. Syrjäsuo, and E. Donovan, pp. 55–60, Univ. of Calgary, Calgary, Alberta, Canada.
- Grocott, A., J. A. Wild, S. E. Milan, and T. K. Yeoman (2009), Superposed epoch analysis of the ionospheric convection evolution during substorms: Onset latitude dependence, *Ann. Geophys.*, *27*, 591–600.
- Henderson, M. G. (2009), Observational evidence for an inside-out substorm onset scenario, *Ann. Geophys.*, *27*, 2129–2140.
- Hiraki, Y. (2013), Stability of Alfvén eigenmodes in the vicinity of auroral arc, *J. Geophys. Res. Space Physics*, *118*, 5277–5285, doi:10.1002/jgra.50483.
- Liang, J., E. F. Donovan, W. W. Liu, B. Jackel, M. Syrjäsuo, S. B. Mende, H. U. Frey, V. Angelopoulos, and M. Connors (2008), Intensification of preexisting auroral arc at substorm expansion onset: Wave-like disruption during the first tens of seconds, *Geophys. Res. Lett.*, *35*, L17S19, doi:10.1029/2008GL033666.
- Motoba, T., K. Hosokawa, A. Kadokura, and N. Sato (2012), Magnetic conjugacy of northern and southern auroral beads, *Geophys. Res. Lett.*, *39*, L08108, doi:10.1029/2012GL051599.
- Raeder, J., P. Zhu, Y. Ge, and G. Siscoe (2013), Auroral signatures of ballooning mode near substorm onset: Open Geospace General Circulation Model simulations, in *Auroral Phenomenology and Magnetospheric Processes: Earth And Other Planets*, edited by A. Keiling et al., pp. 389–395, AGU, Washington, D. C., doi:10.1029/2011GM001200.
- Roux, A., O. Le Contel, D. Fintaine, P. Robert, J. A. Sauvaud, and A. N. Fazakerley (2006), Substorm theories and Cluster multi-point measurements, in *Proceedings of ICS-8*, edited by M. Syrjäsuo, and E. Donovan, pp. 263–268, Univ. of Calgary.
- Sakaguchi, K., K. Shiokawa, A. Ieda, R. Nomura, A. Nakajima, M. Greffen, E. Donovan, I. R. Mann, H. Kim, and M. Lessard (2009), Fine structures and dynamics in auroral initial brightening at substorm onsets, *Ann. Geophys.*, *27*, 623–630.
- Voronkov, I., E. Friedrich, and J. C. Samson (1999), Dynamics of the substorm growth phase as observed using CANOPUS and SuperDARN instruments, *J. Geophys. Res.*, *104*, 28491–28505, doi:10.1029/1999JA900362.
- Wescott, E. M., H. C. Stenbaek-Nielsen, T. N. Davis, W. B. Murcray, H. M. Peek, and P. J. Bottoms (1975), The L = 6.6 Oosik barium plasma injection experiment and magnetic storm of March 7, 1972, *J. Geophys. Res.*, *80*, 951–967, doi:10.1029/JA080i007p00951.